A Variable Insulation System With Potential Application in Cold Climate Greenhouses

Angel Valerio[1], Michele Mossman[*2], Deborah Henderson[3] and Lorne Whitehead[4]

[1,2,4]Department of Physics and Astronomy, The University of British Columbia, 6224 Agricultural Road, Vancouver, Canada
[3]Institute for Sustainable Horticulture, Kwantlen Polytechnic University, 12666 72nd Avenue - Surrey, Canada

[1]angel.valerio.ubc@gmail.com; [*2]michele.mossman@ubc.ca; [3]deborah.henderson@kpu.ca; [4]lorne.whitehead@ubc.ca

***Abstract*- Greenhouse structures are widely used to enable sheltered plant growth. However, traditional transparent greenhouse structures are generally only used in moderate climates because the cost of the energy required for heating in cold climates is prohibitively high. This paper describes a new approach to the design trade-off between light transmission and thermal insulation in greenhouse structures. Here, a low power variable insulation system combining sunlight-concentrating structures and low cost thermal insulation is shown to be a potentially practical solution. Experimental devices have achieved thermal insulation values exceeding 3.33 m^2K/W (compared to 0.42 m^2K/W for triple layer polycarbonate greenhouses) while also maintaining light transmittance values greater than 70%.**

Keywords- Variable Thermal Insulation; Compound Parabolic Concentrator; Light Valve; Cold Climate Greenhouses

I. INTRODUCTION

Cold climate greenhouse growers are forced to increase the insulation of their greenhouses and/or to invest significant amounts of energy to maintain adequate temperature levels for plant growth during the winter season [1, 2]. In most climates, heating typically represents a considerable fraction of the overall operational expenses for commercial greenhouses [3], so it is desirable to increase the thermal insulation of the structure while maintaining adequate light transmission. The ideal greenhouse in sunny but cold climates has two fundamental characteristics: (1) it is highly thermally insulated when the available solar radiation is insufficient for plant growing, and (2) its sunlight transmission is optimal when sufficient sunlight is available [4].

Recently, there has been increased interest in finding a practical solution to improve the low thermal energy performance of current greenhouse structures. Some approaches include movable insulation blocks that expose transparent surfaces [5], panels with multiple layers of transparent materials [6], thermal curtains [7], systems that inject foam [8, 9] or soap bubbles [10] into a gap between two sealed glass surfaces, and completely automated indoor greenhouses [11]. There are a number of reasons why these approaches have not been widely implemented, including the excessive amount of labor required to operate them, high capital investment, high maintenance requirements and limited lifetime. This paper discusses a new approach using a variable insulation system that combines optical concentrators and low cost thermal insulation. The system switches between its light transmissive and thermally insulated states by means of a simple two-state mechanism [12], as described in the following section.

II. THE LIGHT VALVE SYSTEM

The proposed variable insulation system, referred to as the "light valve" system, is depicted in Fig. 1. It is shown in its light transmissive state in Fig. 1a. In this state, highly reflective rotating light valve elements are positioned to permit efficient transmission of sunlight. As shown in Fig. 1b, to achieve the highly thermally insulated state, the light valve elements are rotated such that the thermally resistive elements form a largely continuous layer of insulation.

As shown in Fig. 1, the geometry of each valve element is formed by four curved surfaces arranged such that the assembly forms a series of optical structures known as compound parabolic concentrators [13]. Sunlight that enters the optical passages reflects from the specially designed curved surfaces, and most of the light is transmitted through the assembly. This key optical characteristic is largely independent of the size of the valve elements. For the purpose of this study, elements with an overall height (G) of approximately 0.4 m and equivalent insulating thickness layer (L) of approximately 0.13 m were found to be appropriate [14].

DOI: 10.5963/IJEE0601001

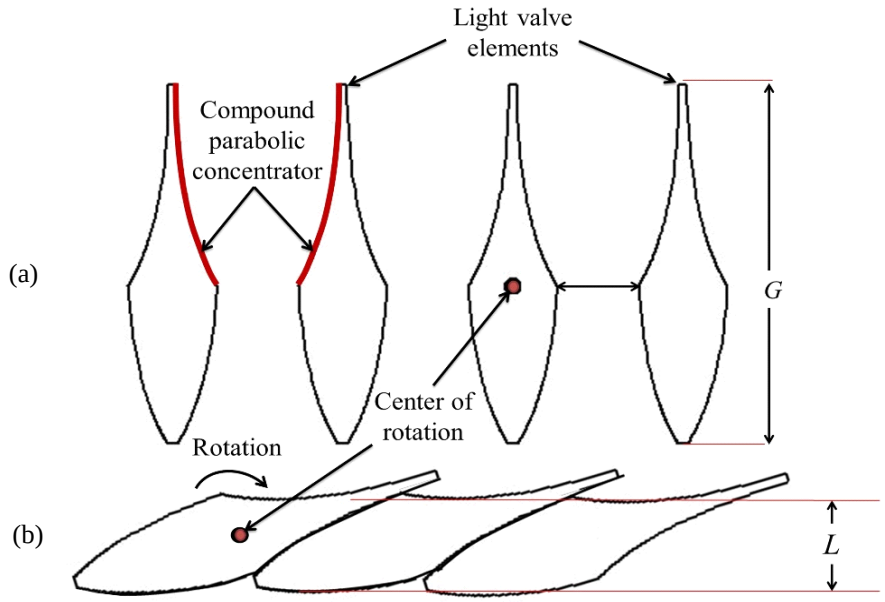

Fig. 1 Section views of the light transmissive (a) and highly thermally insulated (b) states of the light valve system

As shown in Fig. 2, an important technical achievement in the light valve design was the successful implementation of a low pressure seal, which prevents the majority of air exfiltration through the light valve structure, reducing thermal loss by air mass heat transfer [14]. Fibreglass batting, depicted in Fig. 2b, was used to construct the low pressure seal of the valve elements (approximately 0.66 m^2K/W or R-3.7 for each inch of material thickness [15]).

In Fig. 2, the rotation mechanism of the light valve system is shown in a light valve device. An electrically controlled mechanical actuator transmits torque to one or more valve elements, which subsequently transfer this torque to the rest of the valve elements by means of a bar mechanism attached to the lower region of the valve elements, as shown in Fig. 2a and Fig. 2b.

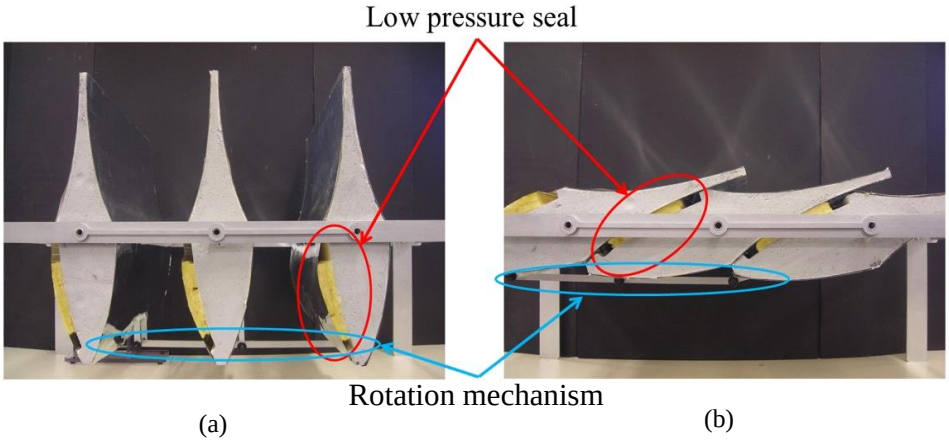

Fig. 2 Sectional view of the (a) light transmissive and (b) thermally insulated states of the light valve experimental device showing the implementation of the low pressure seal and rotation mechanism

III. Modelling The Thermal Resistance Characteristics

In order to determine the thermal resistance characteristics of the assembly, a conceptual model of the heat transfer interactions in the experimental apparatus was developed [14]. This model considers three thermal masses: (1) the light valve structure, (2) the air contained in the light valve device and (3) the water used as a known thermal mass. The thermal model can be thought of as an analogy to an electrical circuit. Basically, the heat flux corresponds to the current in a circuit, the temperature difference corresponds to the potential difference, the thermal resistance corresponds to the electrical resistance, the heat capacity of a material corresponds to the electrical capacitance, Ohm's law corresponds to Fourier's law of heat transfer, and the circuit reduction techniques used for electric circuits apply [16]. In this model, the heat flux between two points is defined as the temperature difference between those points divided by the thermal resistance.

DOI: 10.5963/IJEE0601001

Fig. 3 shows the simplified thermal circuit used for the model, where T_x represents average absolute temperatures (measured in units of K), R_x thermal resistances (in K/W), Q_{ex} heat losses by exfiltration (in W), Q_{swr} short wavelength radiation heat transfers (in W), Q_{lwr} long wavelength radiation heat transfers (in W), K_x heat capacities of the thermal mass systems (in J/K) and I_{sol} is the horizontal irradiance measured on top of the experimental device (in W/m^2). Equations 6-8 represent the energy balances of the three thermal mass systems studied: containers with hot water, air contained in the experimental device and the structure of the experimental device, denoted by subscripts "w", "air" and "st" respectively.

Energy flux is defined to be positive for the energy leaving the mass system and negative for the energy entering the system. As shown in Fig. 3, two heat fluxes define the energy balance of the hot water thermal mass in Eq. 1: the equivalent long wavelength radiation heat transfer from the hot water thermal mass to the experimental device structure ($Q_{lwr,w,st}$), and the heat transfer from the hot water thermal mass to the air contained in the experimental device ($Q_{w,air}$). Three heat fluxes define the energy balance of the air contained in the experimental device as shown in Eq. 2: the heat transfer from the hot water thermal mass to the air contained in the experimental device ($Q_{w,air}$), the heat transfer from the air contained in the experimental device to the experimental device structure ($Q_{air,st}$) and the air exfiltration heat losses (Q_{ex}). Likewise, the thermal balance of the experimental device structure mass system in Eq. 3 is defined by the equivalent heat transfer from the structure to the surroundings ($Q_{out,eq}$), the equivalent long wavelength radiation heat transfer from the hot water thermal mass to the experimental device structure ($Q_{lwr,w,st}$) and the heat transfer from the air contained in the experimental device to the experimental device structure ($Q_{air,st}$).

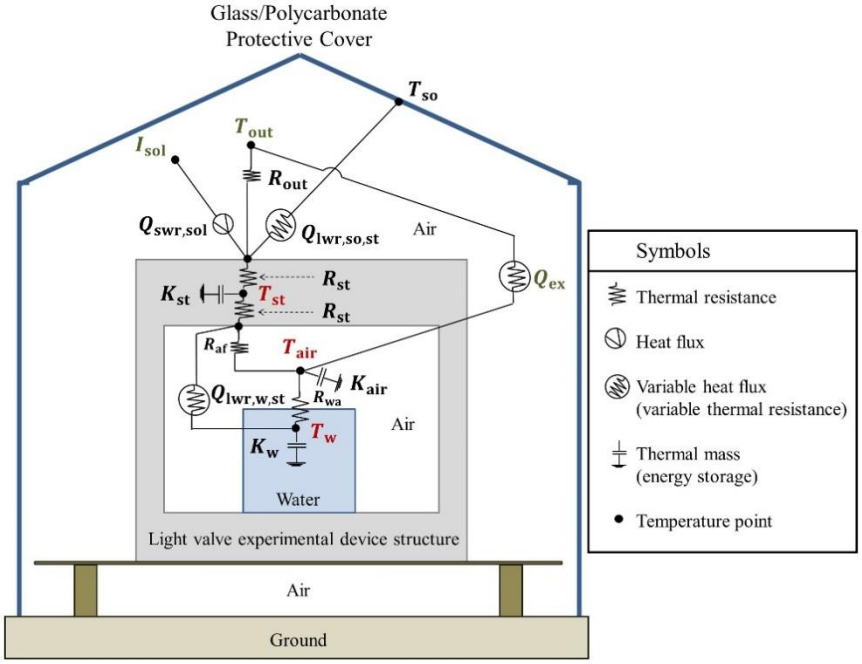

Fig. 3 Thermal resistance model for the light valve experimental apparatus

$$K_{\mathrm{w}}\frac{\mathrm{d}T_{\mathrm{w}}}{\mathrm{d}t} = Q_{\mathrm{lwr,w,st}} + Q_{\mathrm{w,air}} \tag{1}$$

$$K_{\mathrm{air}}\frac{\mathrm{d}T_{\mathrm{air}}}{\mathrm{d}t} = Q_{\mathrm{air,st}} - Q_{\mathrm{w,air}} - Q_{\mathrm{ex}} \tag{2}$$

$$K_{\mathrm{st}}\frac{\mathrm{d}T_{\mathrm{st}}}{\mathrm{d}t} = Q_{\mathrm{out,eq}} - Q_{\mathrm{lwr,w,st}} - Q_{\mathrm{air,st}} \tag{3}$$

Assuming that the only effect of the resulting internal energy variations defined by the energy balance equations 1-3 are temperature differences in the three thermal mass systems, the time-dependent temperatures of the mass systems can be approximated by solving those energy balances for n discrete time periods (Δt). For the specific case of the model presented in this section, the duration of each time period is five minutes (Δt = 300 s). The heat capacity of each thermal mass system (K_x) is defined as the product of its specific heat capacity (c_x), volume (V_x) and density (ρ_x). The temperatures of the three thermal mass systems at time t can be calculated using Equations 4-6. Eq. 4 applies to the containers filled with hot water (T_{w_n}), Eq. 5 applies to the air contained in the experimental device (T_{air_n}) and Eq. 6 applies to the experimental device structure at the middle plane between its outside and inside surfaces (T_{st_n}).

DOI: 10.5963/IJEE0601001

$$T_{\mathrm{w}n} = T_{\mathrm{w}n-1} + \frac{Q_{\mathrm{lwr,w,st}_{n-1}} + Q_{\mathrm{w,air}_{n-1}}}{c_{\mathrm{w}} V_{\mathrm{w}} \rho_{\mathrm{w}}} (\Delta t) \quad (4)$$

$$T_{\mathrm{air}n} = T_{\mathrm{air}n-1} + \frac{Q_{\mathrm{air,st}_{n-1}} - Q_{\mathrm{w,air}_{n-1}} - Q_{\mathrm{ex}}}{c_{\mathrm{air}} V_{\mathrm{air}} \rho_{\mathrm{air}}} (\Delta t) \quad (5)$$

$$T_{\mathrm{st}n} = T_{\mathrm{st}n-1} + \frac{Q_{\mathrm{out,eq}_{n-1}} - Q_{\mathrm{lwr,w,st}_{n-1}} - Q_{\mathrm{air,st}_{n-1}}}{c_{\mathrm{st}} V_{\mathrm{st}} \rho_{\mathrm{st}}} (\Delta t) \quad (6)$$

The conductive and convective heat transfer mechanisms were modelled using the unidimensional Fourier's law [16]. In the case of long wavelength radiation heat transfer, the equivalent long wavelength radiation thermal resistance as defined in Eq. 7 was used for the case of a body with a surface temperature T_1 completely surrounded by a body with a temperature T_2 [16]. R_r is the effective radiation thermal resistance, A is the surface area of the radiation emission body, ε is the emissivity of the body with surface temperature T_1 and σ is the Stefan–Boltzmann constant (σ = 5.67 x 10^{-8} W/m^{2}K^4). For the purposes of the model described in this section, the emissivity of all long wavelength radiation emitting surfaces was assumed to be constant as a function of wavelength [17, 18]. The air exfiltration heat losses (Q_{ex}) were calculated by using Eq. 8, where ΔP_{air} and ΔT_{air} are the pressure and temperature differences of the air inside and outside the experimental device, assuming that the Stack effect is the main air exfiltration mechanism [19-21]. X_{st} is the air conductance of the experimental apparatus, which was measured to be 2.5 x 10^{-4} m^3/sPa for the experiment described in Section 5.1.

$$R_{\mathrm{r}} = \frac{1}{A\left[\varepsilon\sigma(T_1 + T_2)\left({T_1}^2 + {T_2}^2\right)\right]} \quad (7)$$

$$Q_{\mathrm{ex}} = X_{\mathrm{st}} \Delta P_{\mathrm{air}} c_{\mathrm{air}} \rho_{\mathrm{air}} \Delta T_{\mathrm{air}} \quad (8)$$

The calculation of the heat transferred from the structure to the surroundings ($Q_{st,out}$) assumes that there is a hypothetical equivalent air temperature ($T_{e,out}$ in Eq. 9), which, in the absence of any radiation heat exchange, results in the same heat flux [22]. In Eq. 9, T_{out} is the air temperature outside the experimental device, α_{st} is the absorbance of the experimental device structure (measured to be 60% for the gray paint used), p_{sol} is the effective portion of the experimental device exposed to sunlight radiation and I_{sol} is the horizontal irradiance measured on the top of the experimental device. h_{out} is the heat transfer coefficient of the external surface of the experimental device (convection and long wavelength radiation) [22], ε_{st} represents the emissivity of the external surface of the experimental device, and $\Delta E_{st,so}$ is the effective long wavelength radiation heat transfer between the external surface of the experimental device and the protective cover. $\Delta E_{st,so}$ is a complex parameter to calculate, considering that the external surface of the experimental device receives radiation not just from the protective cover but from surrounding objects and the ground as well. The ASHRAE manual [22] provides guidance on the selection of this parameter for diverse scenarios.

$$T_{\mathrm{e,out}} = T_{\mathrm{out}} + \frac{\alpha_{\mathrm{st}} p_{\mathrm{sol}} I_{\mathrm{sol}}}{h_{\mathrm{out}}} - \frac{\varepsilon_{\mathrm{st}} \Delta E_{\mathrm{st,so}}}{h_{\mathrm{out}}} \quad (9)$$

IV. Modeling the Light Transmittance Characteristics

To determine the light transmittance characteristics of the assembly, a model to predict the light transmission of the experimental apparatus was developed based on the light valve ray tracing optical transmittance predictions previously reported [23]. The light transmittance of the light valve system was studied using Monte Carlo ray tracing simulation. This simulation uses ray sources, which generate random rays. As the rays interact with the optical devices, the ray path is determined by the probability of absorption, reflection, transmission, diffraction, refraction and scattering at each interaction. The light transmittance calculation model is described in further detail in a previous publication [23]. This model takes into account the optical losses caused by the greenhouse structural elements as well as the diffuse and direct sunlight transmission in the system based on the expected direct and diffuse radiation contributions of the incident sunlight [24]. The model uses a solar geometry calculation [25] to define two projections of the solar elevation angle on perpendicular planes of the experimental apparatus. The angle θ is the solar elevation projection onto the plane where the light valve profiles are contained, those profiles are shown in Fig. 1, and the angle γ is the projection of the solar elevation onto the perpendicular plane [23], as depicted in Fig. 4.

DOI: 10.5963/IJEE0601001

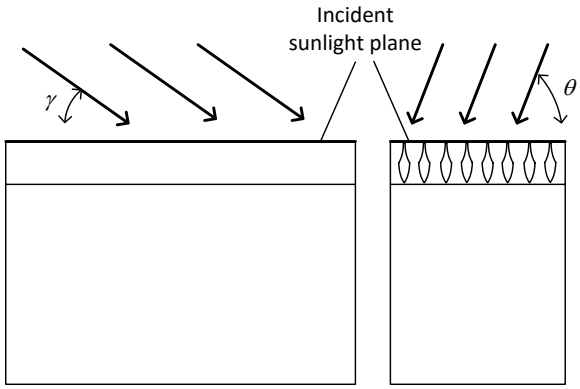

Fig. 4 Front and side views of experimental apparatus showing solar elevation angles γ and θ

The projected angles were used to infer a global optical transmittance value (T_{global}) as a function of the direct ($T_{direct}(\theta,\gamma)$) and diffuse ($T_{diffuse}(\theta)$) transmittance for each experimental data point, as shown in Eq. 10, where x is the percentage diffuse radiation contribution calculated by the Solis model [24]. The optical transmittance value predicted by the model (T_{global}) is then multiplied by the ambient irradiance measured on the top of the experimental device to calculate the intensity of the light that is transmitted into the experimental apparatus.

$$\mathrm{T_{global}} = (1-x)\mathrm{T_{direct}}(\theta,\gamma) + x\mathrm{T_{diffuse}}(\theta) \tag{10}$$

The light transmittance of the diffuse component of the incident solar radiation ($T_{diffuse}(\theta)$) is solely determined by the angular rotation of the light valve elements, which is a function of the solar elevation projection angle θ as previously reported [23]. For this experiment, the direct radiation transmittance ($T_{direct}(\theta,\gamma)$) is a function of the direct radiation transmittance of the light valve system, which is, in turn, a function of the solar elevation projection angle θ (reported in previous communications [23]), and the direct radiation light blockages by the light valve and greenhouse structural elements as a function of the solar elevation projection angle γ. Both T_{direct} and $T_{diffuse}$ are complex functions that cannot be expressed in closed form. However, they have the following broad characteristics: $T_{diffuse}$ has a maximum value of θ=90 ° and decreases monotonically as θ decreases, and T_{direct} has a maximum value of γ=90 ° and θ=90 °, and drops to zero as γ approaches 0 ° and decreases monotonically as θ decreases.

V. Experimental Measurements

Two independent experiments were carried out to verify the thermal resistance and optical transmittance values for the light valve system. In this section, the experimental tools and methods used for those experiments are described.

A. Measuring the Thermal Resistance

The experimental apparatus used to verify the thermal resistance consisted of a rectangular chamber 1.7 m long, 1.1 m wide and 1.1 m high, as depicted in Fig. 5. The side walls and base of the chamber were made from 0.15 m thick polystyrene foam insulation. The experimental light valve system was positioned on the top of the chamber and maintained in the closed or thermally insulating state. The air temperature inside the chamber was increased to a known initial temperature by placing containers filled with hot water inside the chamber. The subsequent decay of the indoor air temperature was measured over time in order to determine the thermal resistance of the light valve system.

The experiment was carried out in two different locations at the University of British Columbia Okanagan (49.93 ° N, 119.39 ° W) and Vancouver (49.26 ° N, 123.25 ° W) campuses. The experimental apparatus was housed inside a transparent structure to protect it against environmental hazards, such as rain and wind. This protective enclosure was a commercially available small greenhouse structure comprised of transparent polycarbonate sheets supported by thin aluminium frame elements. The foam parts of the valve element profiles, light valve module and thermally insulated chamber were cut from expanded polystyrene foam using a computer-controlled hot wire. The material used to coat the valve elements was a 90% specular reflective aluminized polyethylene film [26, 27]. The same 90% reflective coating material was used to line the inner surfaces of the East and West walls of the highly insulated light valve foam box [28], and the South and North walls were coated in diffuse reflective white paint. Four 0.02 m^3 containers of hot water were positioned inside the chamber in order to achieve an initial interior air temperature of 40 ℃.

DOI: 10.5963/IJEE0601001

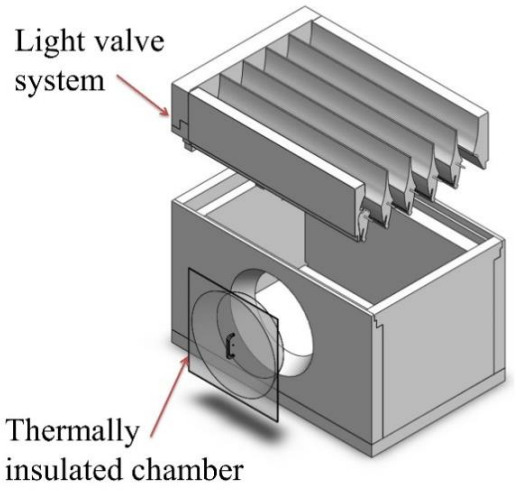

Fig. 5 Computer aided model of the light valve experimental device

The actuator used to rotate the valve elements from its light transmissive to its highly insulating state was a 12V compact DC gear-motor (5.5 Nm at 0.6 RPM). The DC gear motor was coupled to the central valve element, and the torque was transmitted by a bar mechanism attached to the lower region of the valve elements as shown in Figs. 2a and 2b. The temperature in the experimental device was measured using precision integrated-circuit temperature sensors (LM61) [29] with a measurement range of -30 ℃ to 100 ℃. The LM61 temperature sensor response is linearly proportional to the temperature, where a maximum uncertainty of ±2 ℃ for the full temperature operation range is recommended by the manufacturer [29]. The temperature sensors were completely shaded for the duration of the experiments in order to prevent solar thermal radiation interference [30]. The solar radiation gain on the experimental apparatus was inferred by measuring the horizontal solar irradiance using a calibrated light to voltage converter (TSL254R) whose response is proportional to the irradiance level [31]. The spectral response of this sensor was optimized for the PAR spectrum [23]. For the purpose of this experiment, the full solar spectrum contributions were inferred by assuming that the PAR spectrum represents 45% of the solar spectrum [32]. The measurements were taken with a data acquisition card model NI USB6008 12Bit controlled by LabView at 10 second intervals, and the average of the measured values was stored in a data file every five minutes.

B. Thermal Experiment Results

Thermal decay experiments were carried out during the period from September 2012 to March 2014. The air temperature in the experimental device (T_{air}) predicted by the thermal model fit well with the experimental observations for the average thermal resistance value of the experimental apparatus structure equal to 4.29 m^2K/W ± 0.15 m^2KW (R-24.4 ± R-0.8). The thermal resistance expected for the light valve experimental apparatus was between 4.25 m^2K/W and 4.89 m^2K/W (R-24.1 to R-27.8), considering the light valve module and the thermally insulated chamber. For this calculation, an average ideal thermal resistance value between 0.73 m^2K/W and 0.84 m^2K/W per inch was assumed for the expanded polystyrene foam [33]. The total thermal resistance value for the 15 cm thick polystyrene foam sheeting was 4.7 m^2K/W.

Using the thermal resistance inferred for the experimental apparatus structure (4.29 m^2K/W ± 0.15 m^2KW), a conservative thermal resistance value was deduced for the light valve module alone between 3.33 m^2K/W and 4.21 m^2K/W (R-18.9 and R-23.9) for the case of an ideal thermally insulated chamber with a thermal resistance value between 0.76 m^2K/W and 0.81 m^2K/W per inch [33]. In Fig. 6, the red dots represent the air temperature measured in the light valve experimental device, the blue dots are the air temperatures measured outside of the experimental device (T_{out}), and the black dashed line is the optimized fit obtained using the thermal model. The average relative difference between the air temperature measured in the experimental device and the one predicated by the thermal model (T_{air}) was 4%.

DOI: 10.5963/IJEE0601001

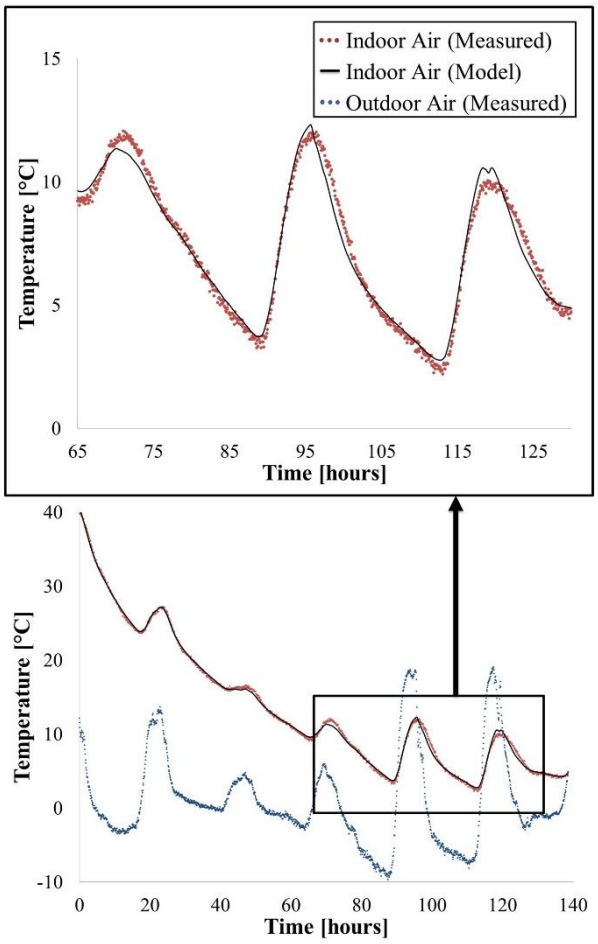

Fig. 6 Thermal decay experiment (February 21 to 27, 2014)

The average values used in the model for the thermal conductance of the air films on the inner and outer surfaces of the experimental device and the water containers were 7 W/m^{2}K, 16 W/m^{2}K and 7 W/m^{2}K, respectively; those values are consistent with those reported by the literature for similar experiments [34-36]. The emissivity value (ε) used for the water containers and the light valve experimental apparatus structure is 0.9, which is consistent with the emissivity values used for thermal models previously reported [37, 38].

C. Measuring the Light Transmittance

The light transmittance through the light valve system has been verified in previous experiments [23]. In the experimental work reported in this paper, the light transmittance of the light valve system was further verified by using a larger scale experimental apparatus installed in an already constructed and fully functional greenhouse. The objectives of this experiment were: (1) to verify the ray tracing light transmittance values previously predicted for the light valve system when operated as a solar tracker [23], and (2) to demonstrate the practicality of scaling up the system and integrating it within a fully functional greenhouse operation. The experimental apparatus was installed at the roof level in a fully functional greenhouse, and a thermally insulated chamber was constructed around the system to isolate that section from the rest of the greenhouse. The light valve modules were equipped with solar tracking capabilities using a customized closed-loop solar tracking control algorithm.

The horizontal solar irradiance was measured both on top of the light valve experimental apparatus and approximately 0.45 m below the light valve modules where the light obstruction by the greenhouse structure and crops was minimized. The ratio of the energy flux above and below the light valve system was reported as the light transmittance value. This light transmittance value was compared to the ray tracing predictions of a customized ray tracing model. The irradiance at the level of the growing trays (1.3 m above ground) was measured at 0.5 meter intervals on the three growing trays contained within the experimental apparatus. The trays were separated by 1.5 m.

DOI: 10.5963/IJEE0601001

(a) (b)

Fig. 7 (a) Photograph of the thermally insulated chamber of the light transmission light valve experimental device at the light transmission experimental location. (b) Photograph of the six light valve modules viewed from below in their light transmissive state

This experiment was conducted in a greenhouse facility at Kwantlen Polytechnic University's Institute for Sustainable Horticulture in Langley, British Columbia (49.11 °N, 122.64 °W). Six light valve modules, each with a total area of 4 m^2 (3.6 m^2 of effective light valve area and 0.4 m^2 of frame area), were constructed using aluminized polyethylene film [27] laminated onto expanded polystyrene foam valve element structures [39]. The six light valve modules were customized to be installed at the roof of the experimental greenhouse structure without disrupting any existing structural elements or services. To achieve this, the original design dimensions of the light valve system were scaled down by 25%. The light valve experimental apparatus included the construction of a 0.1 m thick insulation chamber, shown in Fig. 7a. Once the enclosure was completed, modules were suspended from the roof using lightweight steel cables, as can be seen in Fig. 7b. The top two thirds of the thermally insulated chamber inner walls were covered with 90% specular reflective mirrors [27], and the remaining wall area was painted with 90% diffuse reflective white paint.

The irradiance measurements were performed using a light-to-voltage linear converter (TSL254R) [31]. Diffuse acrylic was used to reduce the angular response sensitivity of the sensor [40], and glass and hot mirrors [41] were used to reduce the ultraviolet and infrared contributions of the incident sunlight limiting the sensor response to the PAR spectrum [40]. A commercial light meter [42] was used for a portion of the experiment. Again, data was taken using the NI-DAQ card (USB6008 12Bit) and LabView at 10 second intervals, and the average of the measured values was stored in a data file every five minutes. The angular position of the light valve elements for solar tracking was independently controlled and monitored by an inexpensive microcontroller [43]. The closed-loop solar tracking control adjusted the angular position of the valve elements once per hour to the appropriate position depending on the solar geometry and a ray tracing optimization by means of a potentiometer feedback connected to a linear actuator [44] [23].

D. Light Transmittance Experiment Results

Figure 8 compares the experimental transmitted PAR irradiance in the light valve system with the ray tracing model predictions. The red dots represent the irradiance measured in the experimental device; the vertical uncertainty reported is the statistical error of the averaging over five minutes of the 0.1 Hz irradiance readings of the light sensor. The solid black line in Fig. 8 represents the predicted irradiance in the experimental device according to the ray tracing model. The determination coefficient of the measured and predicted data was calculated to be 0.84.

The light transmittance value of the experimental device depends on the solar elevation, and it varies with the position of the sun during the day [23]. The three highest hourly average light transmittance values (average of the ratio of the transmitted over the ambient irradiance over the course of an hour) measured with the experimental apparatus were 0.483 ± 0.129 (from 10 am to 11 am), 0.541 ± 0.106 (from 11 am to 12 pm) and 0.311 ± 0.137 (from 12 pm to 1 pm) under predominantly clear sky conditions from February 19 to 21, 2014 and from February 25, 26 and 28, 2014. Those measurements compared well with the predicted transmittance values from the ray tracing model for the same data points, which were 0.516 ± 0.036 (from 10 am 11 am), 0.537 ± 0.018 (from 11 am to 12 pm) and 0.459 ± 0.027 (from 12 pm to 1 pm). Selected data points from 10:50 am to 11:05 am and 11:30 am to 11:45 am were not taken into account in the calculations because of atypically high irradiance measurements caused by an inadvertent localized concentration of sunlight. A rapid and uncharacteristic decrease of the irradiance values in the experimental device was observed from 12:00 pm to 12:20 pm during predominantly clear days (and

DOI: 10.5963/IJEE0601001

until 12:50 pm on February 25, 2014). This decrease was caused by partial shading by the structural elements in the greenhouse on the transmitted irradiance sensor, so these data points were not included in the analysis.

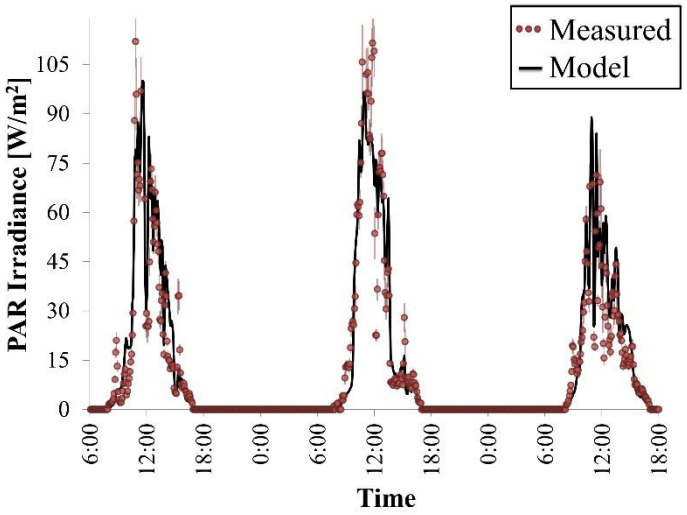

Fig. 8 Comparison of the irradiance measurements in the light valve experimental device and the predictions of the ray tracing model [23] measured 0.45 m below the light valve modules from February 19 to 21, 2014. The graph shows measured values at red dots, compared to the calculated model values, which are plotted as a solid black line.

The horizontal irradiance of the light valve experimental device at the level of the plant growth tray (1.3 m above the ground) was also measured on August 20 and August 21, 2013 (totally clear sky days) at 11:30 am. The average measured irradiance value for the experimental device was 107 PAR W/m^2 ± 11 PAR W/m^2, which is in agreement with the irradiance value predicted by the ray tracing model for the same days and time (114 PAR W/m^2). This irradiance value at the growing tray level is higher than the critical point where the light intensity is a limiting factor for photosynthesis under ambient CO2 concentrations (about 100 PAR W/m^2) [45].

The transmittance values achieved in the experimental device were lower than what would be achieved in an ideal installation where the light valve system is properly tilted and east-west aligned and the structural blockages are minimized. It is expected that in more suitable installation conditions, the light transmittance could exceed 70% for direct radiation under most solar elevations based on previously reported ray tracing studies of the light valve system working as a solar tracker [23]. While the experimental set-up used in this experiment was not ideal, the results obtained by it are meaningful because they verified that the ray tracing model more than adequately predicts the optical behaviour of the light valve system and that the light valve design can be implemented in a real world greenhouse situation.

VI. Discussion of the Results

The most important achievement of the light valve design is that the optical and thermal responses are largely decoupled, providing a practical solution to maintain proper light transmission through the greenhouse structure while reducing the energy used for heating. This characteristic can be described in terms of the Pareto optimal frontier, a multi-objective optimization in which a particular set of optimal solutions is used to define design limits for two or more correlated and contrasting parameters [46]. Figure 9 compares the Pareto frontier of the thermal and optical performance of the light valve design discussed in this paper to that of present-day polycarbonate windows typically used in greenhouses. In the case of the polycarbonate windows, increasing the number of material layers causes an increase in the overall thermal resistance. Quadruple layer polycarbonate covers have light transmittance values above 65% (at normal light incidence angle) and thermal resistance values above 0.50 m^{2}K/W (R-2.9) [47], and, for the purposes of the project discussed in this paper, are considered to be the practical limit for polycarbonate windows.

As shown in Fig. 9, the light valve design does not just move the Pareto optimal frontier, but largely decouples the light transmittance from the thermal insulation of the structure [23]. Consequently, high thermal insulation values can be obtained using the light valve design while maintaining an average direct radiation optics performance above 70% for most solar elevations (above 80% transmittance at normal light incidence angle) [23].

DOI: 10.5963/IJEE0601001

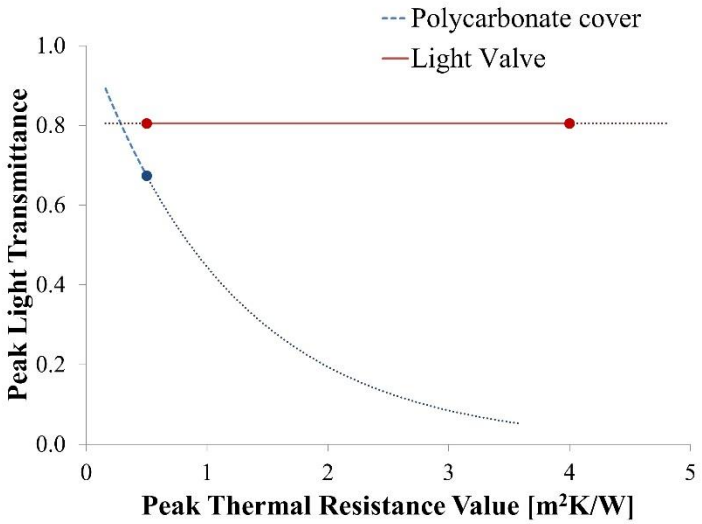

Fig. 9 Thermal resistance and optical transmittance at the normal light incidence angle of polycarbonate windows and the light valve design are compared using Pareto optimal frontiers [23]. The dotted portion of the lines represents the region that is not practical for greenhouse farming applications [23].

This paper reports the research results for an early prototype of this light value technology. Given that this device has not yet been developed into a commercial product, it is premature to specify the exact overall cost. However, a preliminary cost analysis has been carried out, and it has been estimated that a product based on this technology could be sold for ~$6-8/sq. ft. At this price, the benefits of the technology could be realized in acceptable payback times of ≤5 years for the capital investment within key target markets, making it a viable option for the greenhouse industry.

VII. CONCLUSION

This paper describes a new approach to substantially reduce the energy required for heating in cold climate greenhouses while conserving appropriate sunlight transmission through the structure. The light valve system can act both as a sunlight transparent window and as a highly thermally insulated ceiling capable of keeping the structure warm during periods of cold weather. The system uses readily available and inexpensive materials, and the switching between the light transmissive and the thermally insulated states can be done with a low-cost rotation device.

It was experimentally verified that the light valve system has acceptable photosynthetically active radiation transmittance values (ideal optical transmittance values are above 70%, and this initial experimental system achieved 84% transmittance) and a thermal resistance value above 3.33 m^2K/W, compared to 0.17 m^2K/W in common glass panels [48, 49]. The experimental devices presented in this document demonstrate the feasibility of the construction of the light valve design using inexpensive and readily available materials, as well as its practicality for installation in a fully functional greenhouse. This technology could be widely used in regions that typically experience cold but sunny winter conditions. On cloudy days, the light valve system will somewhat reduce the overall light transmission compared to a standard transparent greenhouse structure, but under most circumstances, the thermal advantages provided by the light valve system will surpass the drawbacks associated with this reduction in overall light transmission. As a result, the light valve system has the potential to expand available farmland to regions whose climates make present-time greenhouse technologies impractical, and to largely decouple greenhouse energy operation costs (heating and lighting) and climatic conditions (ambient temperature), thereby expanding the productive season.

ACKNOWLEDGMENT

The authors gratefully acknowledge financial support from the Natural Sciences and Engineering Research Council of Canada and the University of British Columbia, as well as the important technical inputs of Jon Scott, Douglas Campbell, Jason Radel, Edson Sanchez, Megan Ogilvie, Andres Torres and John Huizinga.

REFERENCES

[1] J. Opdam, G. Schoonderbeek, E. Heller, and A. De Gelder, Closed greenhouse: a starting point for sustainable entrepreneurship in horticulture, pp. 517-524, 2004.

[2] A. Monteiro, Greenhouses for mild-winter climates: goals and restraints, pp. 21-32, 1988.

[3] G. Ntinas, P. Kougias, and C. Nikita-Martzopoulou, Experimental performance of a hybrid solar energy saving system in greenhouses, International Agrophysics, 25, 2011.

[4] D. G. Hessayon, The greenhouse expert, Sterling Publishing Company, Inc., 1994.

[5] B. Norton, Harnessing Solar Heat, Springer, 2014.

[6] E. M. Abdel-Bary, M. N. Ismail, A. A. Yehia, and A. A. Abdel-Hakim, Recycling of polyethylene films used in greenhouses—

DOI: 10.5963/IJEE0601001

Development of multilayer plastic films, Polym. Degrad. Stab. 62, pp. 111-115, 1998.

[7] S. Cohen, and M. Fuchs, Measuring and predicting Radiometric Properties of Reflective Shade Nets and Thermal Screens, J. Agric. Eng. Res. 73, pp. 245-255, 1999.

[8] K. Aberkani, A. Gosselin, M. Dorais, and S. Vineberg, Effects of insulating foams between double polythylene films on light transmission, growth and productivity of greenhouse tomato plants grown under supplemental lighting, pp. 449-454, 2005.

[9] J. Villeneuve, D. De Halleux, A. Gosselin, and D. Amar, Concept of dynamic liquid foam insulation for greenhouse insulation and the assessment of its energy consumption and agronomic performances, pp. 605-610, 2004.

[10] H. J. Han, Y. I. Jeon, S. H. Lim, W. W. Kim, and K. Chen, New developments in illumination, heating and cooling technologies for energy-efficient buildings, Energy, 35, pp. 2647-2653, 2010.

[11] Urban Barns, Urban Barn designs and manufactures modular indoor greenhouses, 2014.

[12] L. Whitehead, Adjustable transmissive insulative array of vanes, system and building structure, PCT/CA2012/050848, 2013.

[13] R. Winston, Principles of solar concentrators of a novel design, Solar Energy, 16, pp. 89-95, 1974.

[14] A. Valerio, Light transmissive variable thermal insulator based on nonimaging optics with potential application in cold climate greenhouses, 2014.

[15] Colorado Energy, R-Value Table, 2014.

[16] F. P. Incropera, Fundamentals of heat and mass transfer, John Wiley & Sons, 2011.

[17] R. G. Driggers, Encyclopedia of optical engineering, CRC press, 2003.

[18] M. Kaviany, Principles of heat transfer, John Wiley & Sons, 2002.

[19] T. Boulard, J. Meneses, M. Mermier, and G. Papadakis, Characterisation of the mechanisms involved in the natural ventilation of greenhouses, pp. 383-398, 1994.

[20] T. Boulard, and A. Baille, Modelling of air exchange rate in a greenhouse equipped with continuous roof vents, J. Agric. Eng. Res. 61, pp. 37-48, 1995.

[21] D. Thorpe, Energy Management in Buildings: The Earthscan Expert Guide, Routledge, 2013.

[22] American Society of Heating, Refrigerating and Air-Conditioning Engineers, Fundamentals Handbook, Atlanta, 1997.

[23] A. A. Valerio, M. A. Mossman, and L. A. Whitehead, Light valve based on nonimaging optics with potential application in cold climate greenhouses, 2014 Proceedings of SPIE Vol. 9191, pp. 91910K-1 to 91910K-15, 2014.

[24] P. Ineichen, A broadband simplified version of the Solis clear sky model, Solar Energy, 82, pp. 758-762, 2008.

[25] J. A. Duffie, and W. A. Beckman, Solar engineering of thermal processes, John Wiley & Sons, 2013.

[26] K. D. Dodson, and T. G. Squires, Polyethylene terephthalate film, 1975.

[27] Nielsen Enterprises, Vapor aluminization deposition specifications sheet, 2014.

[28] TAP Plastics, Mirrored Acrylic Sheets, 2014.

[29] Texas Instruments, LM61 2.7V, SOT-23 or TO-92 Temperature Sensor, 2014.

[30] J. M. Tarara, and G. A. Hoheisel, Low-cost shielding to minimize radiation errors of temperature sensors in the field, Horticultural Science, 42, 2007.

[31] Austria MicroSystems, TSL254 Light-to-Voltage, High sensitivity sidelooker package, 2014.

[32] J. F. Escobedo, E. N. Gomes, A. P. Oliveira, and J. Soares, Ratios of UV, PAR and NIR components to global solar radiation measured at Botucatu site in Brazil, Renewable Energy, 36, pp. 169-178, 2011.

[33] AFM, EPS Foam Type II technical data, 2014.

[34] B. J. Taylor, and M. S. Imbabi, The effect of air film thermal resistance on the behaviour of dynamic insulation, Build. Environ. 32, pp. 397-404, 1997.

[35] J. Yu, L. Tian, C. Yang, X. Xu, and J. Wang, Optimum insulation thickness of residential roof with respect to solar-air degree-hours in hot summer and cold winter zone of china, Energy Build. 43, pp. 2304-2313, 2011.

[36] R. Dylewski, and J. Adamczyk, Economic and environmental benefits of thermal insulation of building external walls, Build. Environ. 46, pp. 2615-2623, 2011.

[37] S. A. Al-Sanea, Thermal performance of building roof elements, Build. Environ. 37, pp. 665-675, 2002.

[38] H. Suehrcke, E. L. Peterson, and N. Selby, Effect of roof solar reflectance on the building heat gain in a hot climate, Energy Build. 40, pp. 2224-2235, 2008.

[39] Foam Control, EPS Foam Type II technical data, 2014.

[40] P. Fielder, and P. Comeau, Construction and testing of an inexpensive PAR sensor.BC Ministry of Forests, Research Branch, Victoria, 2000.

[41] Edmund Optics, Hot Mirrors, 2014.

[42] Konica Minolta, TL-1 Illuminance Meter, 2014.

[43] Arduino, Arduino Mega ATmega1280, 2015.

[44] WuXi, 12V Linear actuator model HB-DJ806, 2014.

[45] J. W. Wilson, D. Hand, and M. Hannah, Light interception and photosynthetic efficiency in some glasshouse crops, J. Exp. Bot. 43, pp. 363-373, 1992.

[46] A. V. Lotov, V. A. Bushenkov, and G. K. Kamenev, Interactive decision maps: Approximation and visualization of Pareto frontier,

DOI: 10.5963/IJEE0601001

Springer, 2004.
[47] CO-EX, Multi-wall (Twin, Triple, Five, X-Strong and M-wall) Polycarbonate Panels from CO-EX Corporation, 2014.
[48] D. Ryan, T. Hinman, Sustainable Season Extension: Considerations for Design, National Center for Appropriate Technology, 2011.
[49] National Glass, Float Glass Manufacture, 2014.

DOI: 10.5963/IJEE0601001